Supporting Information

Figure S1. (a-c) Top view representations of Li_2S_4 diffusion pathways on the M-Nb_2O_5 (001) surface and (d) the corresponding energy profile.

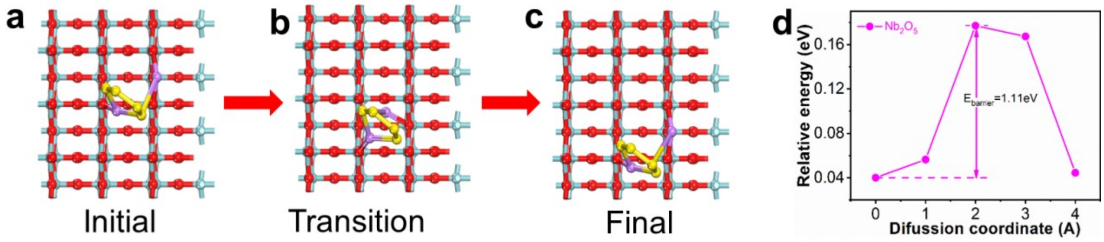

Note: The cyan, red, purple and yellow spheres represent Nb, O, Li, and S, respectively.

Figure S2. Digital photos of the typical Nb_2O_5-NbC/CNF-PS: (a) the multilayer-folded. (b) the bended.

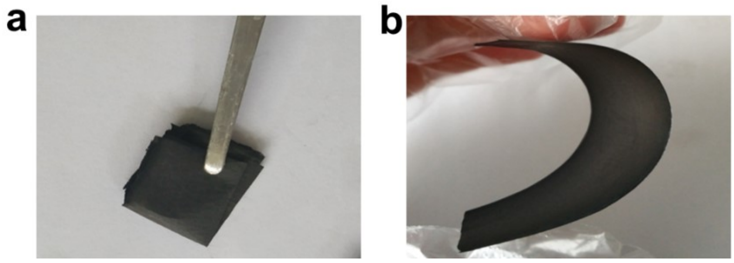

Figure S3. SEM (a, b) and TEM (c) images of the pure CNF.

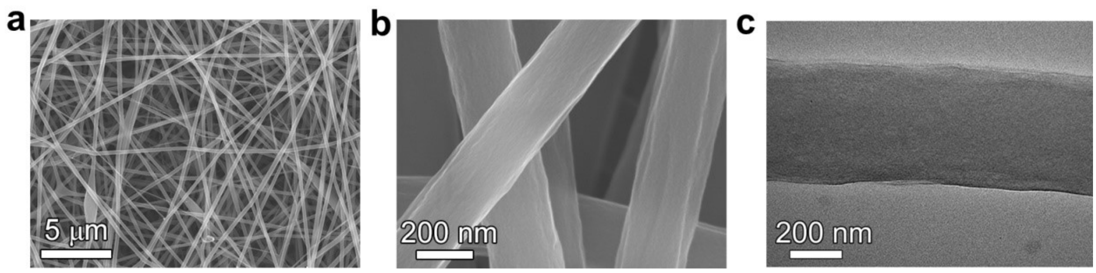

Figure S4. SEM images of the Nb_2O_5-NbC/CNF.

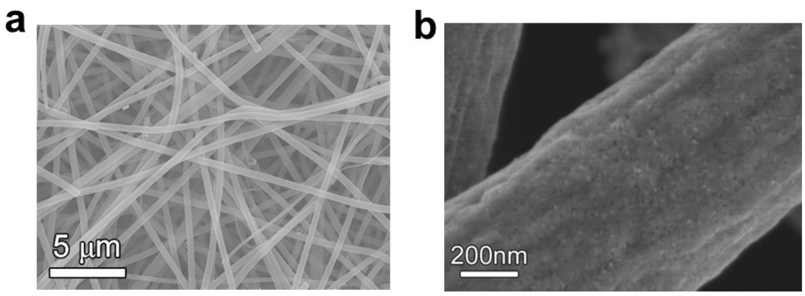

Figure S5. SEM images of the typical Nb_2O_5-NbC/CNF-PS.

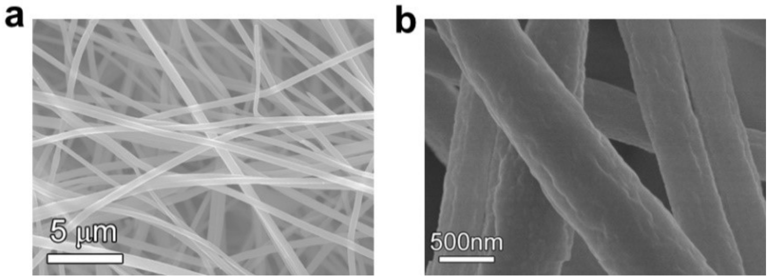

Figure S6. XRD patterns. (a) Nb_2O_5-NbC/CNF-PS pyrolized at 900°C or 1000°C. (b) Nb_2O_5-NbC/CNF pyrolized at 900°C or 1000°C.

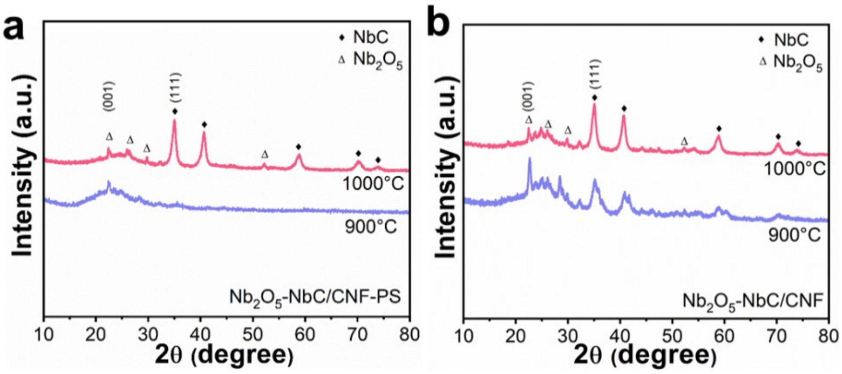

Figure S7. XPS of the typical Nb_2O_5-NbC/CNF-PS and Nb_2O_5-NbC/CNF without PS.

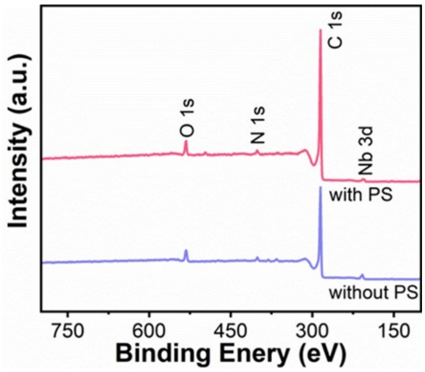

Figure S8. Pore size distribution plots of the typical Nb_2O_5-NbC/CNF-PS and Nb_2O_5-NbC/CNF without PS.

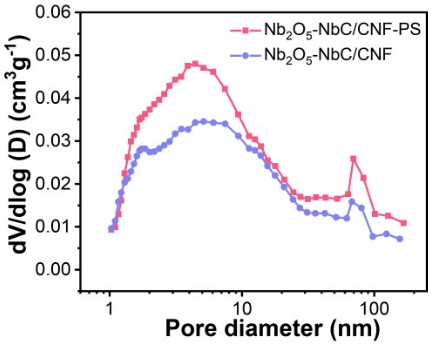

Figure S9. TG plot of the C/S composite.

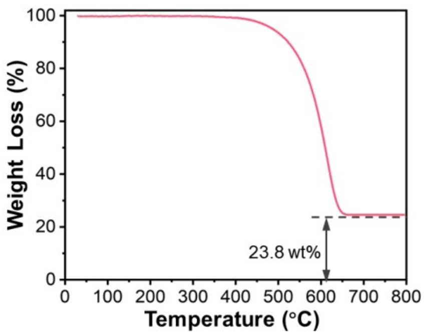

Figure S10. SEM (a, b), TEM (c) images and XRD pattern of the Nb_2O_5-NbC(L)/CNF-PS.

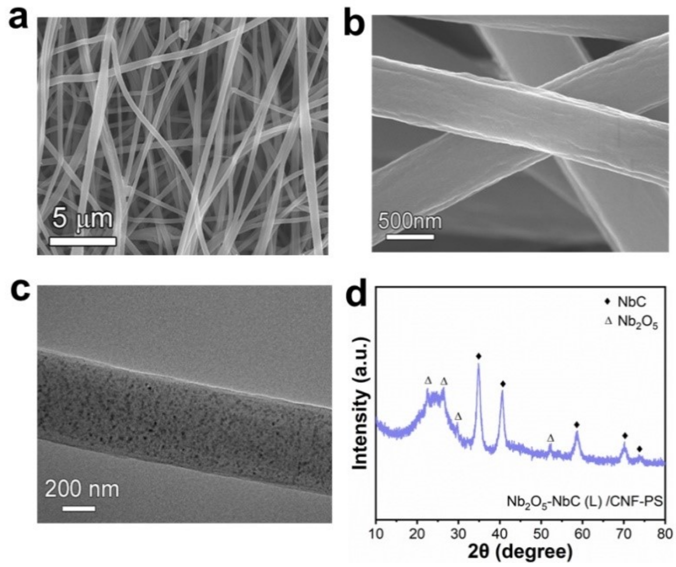

Figure S11. Electrochemical performance of the Li–S batteries with Nb_2O_5-NbC(L)/CNF-PS. (a) Cycle stability, (b)Rate, and (c)The discharge-charge profiles.

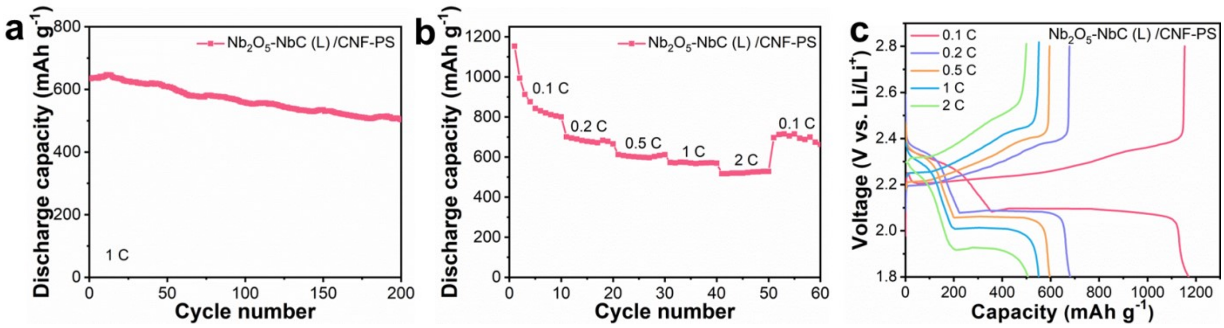

Figure S12. Cycle stability of the Li–S batteries without an interlayer.

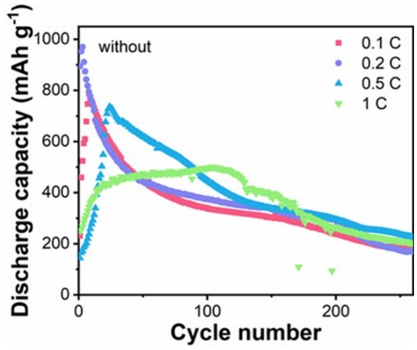

Figure S13. The discharge-charge profiles of the batteries with (a) the typical Nb_2O_5-NbC/CNF-PS (b) Nb_2O_5-NbC/CNF and (c) CNF.

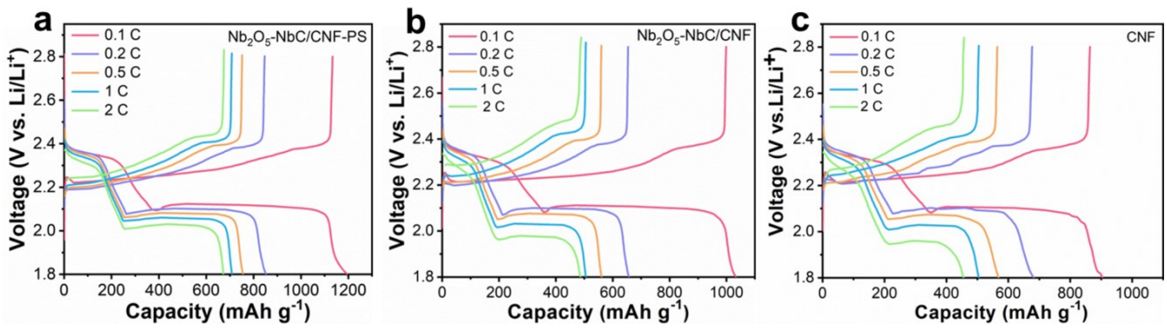

Figure S14. SEM images after 100 cycles: Sulfur cathode (a) without and (b) with the typical Nb_2O_5-NbC/CNF-PS, lithium anode (c) without and (d) with the typical Nb_2O_5-NbC/CNF-PS.

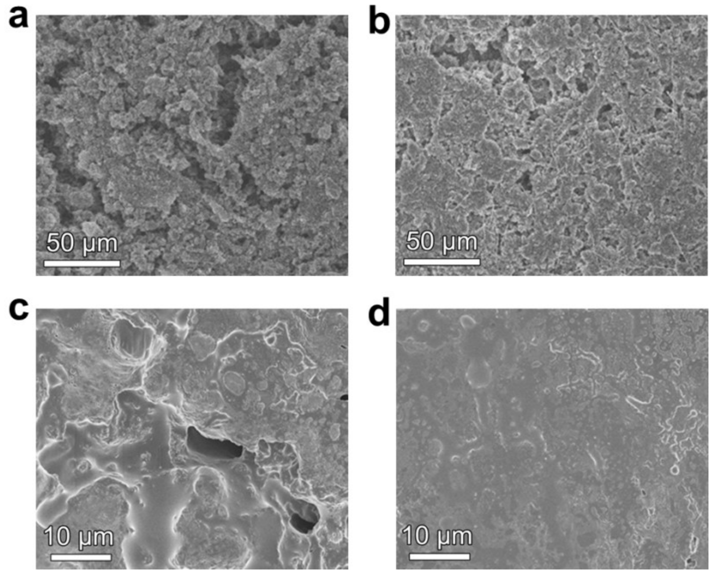

Figure S15. Electrochemical impedance spectroscopy (EIS) plots of Li–S batteries.

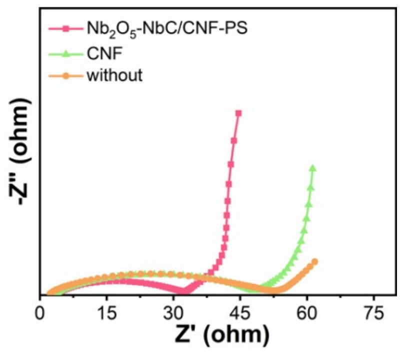

Figure S16. CV curves of Li-S batteries at various scan rates. (a) with CNF interlayer (b) without interlayer.

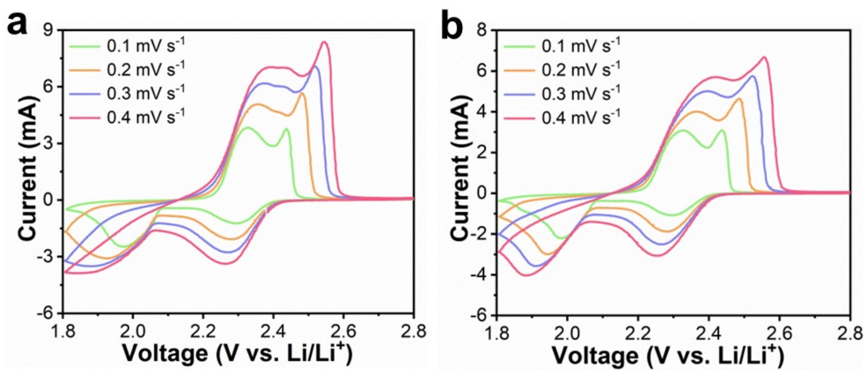

Figure S17. CV curves of the symmetric cell employing Nb_2O_5-NbC/CNF-PS or CNF as electrode.

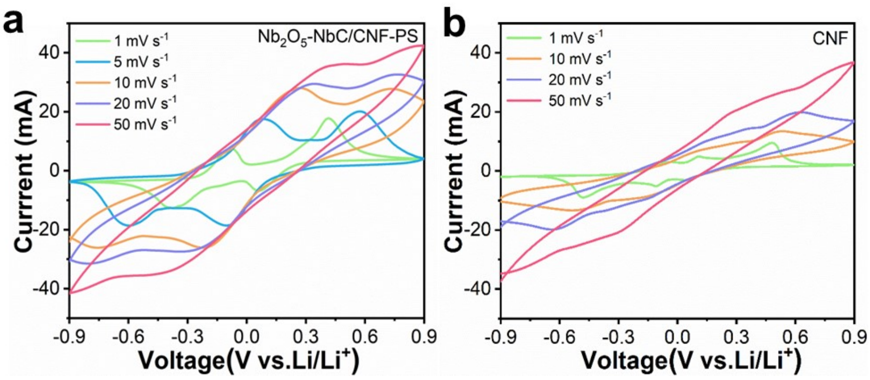

Table S1. The adsorption energy of the representive LiPSs on the optimized configurations of Nb_2O_5 or NbC.

	Optimized configurations	$E_{adsorption\ energy}$ towards Li_2S_6 (eV)	$E_{adsorption\ energy}$ towards Li_2S_4 (eV)
Nb_2O_5-O	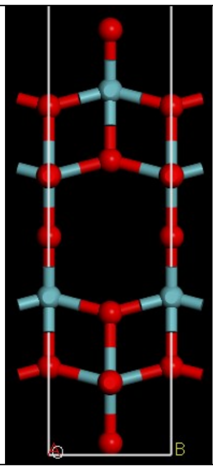	-5.13	-6.07
NbC-C	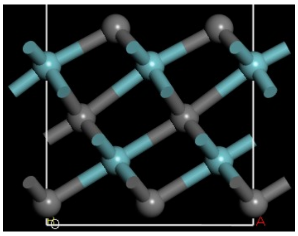	-4.14	-5.94

Table S2. Conductivity of different samples measured by the four-point probe method.

Samples	Nb_2O_5-NbC/CNF-PS	CNF
Conductivity（S cm^{-1}）	1.42×10^{-2}	3.13×10^{-3}

Table S3. Measured BET Surface Area, and the Pore Volume of different samples.

Samples	BET surface area (m^2 g^{-1})	Micropore volume (cm^3 g^{-1})	Mesopore volume (cm^3 g^{-1})	Total pore volume (cm^3 g^{-1})
Nb_2O_5-NbC/CNF-PS	62.63	0.013	0.074	0.087
Nb_2O_5-NbC/CNF	29.37	0.0098	0.045	0.055

Table S4. The slope of the curve (I_p/$v^{0.5}$).

Samples	C1	C2
Nb_2O_5-NbC/CNF-PS	0.38177	0.25608
CNF	0.18363	0.19771
Without interlayer	0.032485	0.13771

The Li ion diffusion constant can be estimated using the Randles-Sevcik equation[1]:

$$I_p = 2.69 \times 10^5 n^{3/2} A D_{Li}^{1/2} v^{1/2} C_{Li} \qquad [1]$$

where I_p is the peak current, n represents electron number, A represents electrode area, D_{Li} is the Li ion diffusion coefficient, C_{Li} is the Li ion concentration in the electrochemical reaction, is the scanning rate.

Table S5. Lithium ion diffusion coefficients.

Samples	D_{Li+} [cm^2 S^{-1}]	
	C1 (cathode peak at 1.8-2.0V)	C2 (cathode peak at 2.1-2.4V)
Nb_2O_5-NbC/CNF-PS	19.69×10^{-8}	8.86×10^{-8}
CNF	4.55×10^{-8}	5.28×10^{-8}
Without interlayer	1.43×10^{-9}	2.56×10^{-8}

Table S6. Electrochemical performance of some representative recently-reported heterostructures-containing interlayer/modified separator in the recently-reported literatures.

Interlayer/ modified separator	Initial capacity (mAh g^{-1})	Rate （C）	Cycles	Capacity Decay ($cycle^{-1}$)	Cycling performance (mAh g^{-1})	Sulfur loading (mg cm^{-2})	Sulfur cathode	Reference
Nb_2O_5-NbC/CNF-PS	**800**	**1**	**800**	**0.044%**	**508.5**	**1.2**	**MC/S***	**This work**
	818	**0.2**	**100**	**——**	**776.4**	**3**		
	752	**0.5**	**250**	**0.045%**	**612**	**4**		
NbN/G modified separator	1079	1	300	0.096%	768	1-1.5	Sulfur	[2]
NCM (NbC-modified separator)	1304	0.2	100	0.24%	988.4	2	Sulfur	[3]
	1082	2	1500	0.037%	500			
MoP_2/CNT interlayer	1223	0.2	100	0.152%	905	1.2	Sulfur	[4]
	1035	0.2	500	——	641	2.8		
	892	1	500	0.045%	392.8			
MoO_2–Mo_2N-SP-Celgard	1083	1	500	0.028%	632.6	0.8-1	CB/S	[5]
	1152	0.1	100	——	790	3.1		
	826	0.2	100	0.26%	590	4		
SnO_2 NWs@CP interlayer	900	0.2	100	——	886	2.2	Sulfur	[6]
	883	0.2	100	——	815	4		

Ni/SiO_2/G-modified separator	1282	0.2	100	0.28%	922	1-1.2	——	[7]
	940	2	300	0.085%	699			
ReS_2@NG interlayer	854	2	800	0.064%	854	1.4-1.6	CNT/S	[8]
	796	1	500	0.036%	398	3.27		
CoS_2/HPGC interlayer	1055	0.2	250	——	846	2.5-3	Sulfur	[9]
	743	1	500	0.07%	519			
TiO_2-TiN modified separator	1034	0.3	300	0.027%	927	1.0-1.2	MWCNTs/S	[10]
TiO-TiO_2/BNCNF interlayer	1014.7	0.5	400	0.092%	637.2	2.5	CMK-3-S	[11]
	650	2	120	——	598			

* MC: mesoporous carbon

Table S7. Electrochemical performance of some representative recently-reported Nb-relative catalysists in the recently-reported literatures.

Host	Initial capacity (mAh g^{-1})	Rate（C）	Cycles	Capacity Decay ($cycle^{-1}$)	Cycling performance (mAh g^{-1})	Sulfur loading (mg cm^{-2})	Reference
Nb_2O_5-NbC/CNF-PS	**800**	**1**	**800**	**0.044%**	**508.5**	**1.2**	**This work**
	818	**0.2**	**100**	**——**	**776.4**	**3**	
	752	**0.5**	**250**	**0.045%**	**612**	**4**	
HCN@NbC/S	813	3	800	0.05%	500	1.5	[12]
	906	0.1	100	0.19%	730	3	
S/NbN@NG	948	1	400	0.09%	592	2.4	[13]
Co-NbN/rGO/S	1103	0.2	150	——	706.5	1.2-1.7	[14]
	984	1	800	0.07%	404.5		
MCM/Nb_2O_5/S	1289	0.5	200	0.14%	913	1.5	[15]
	1196	2	500	——	650		
NbS_2@S@IG	881	0.5	350	0.07%	856	1.05	[16]
	515	1	600	——	405	3.25	
S–A/T-Nb_2O_5	1279	0.1	100	——	1006	1.5	[17]
	902	0.5	800		600		
A-Nb_2O_{5-x}@MCS-S	902.5	0.2	500	——	615	1	[18]
	1126	1	1200	0.024%	746.3		

References

[1] H. Kim, J. Lee, H. Ahn, O. Kim, M.J. Park, Synthesis of three-dimensionally interconnected sulfur-rich polymers for cathode materials of high-rate lithium-sulfur batteries, Nat. Commun., 6 (2015) 7278.

[2] H.F. Shi, Z.H. Sun, W. Lv, S.J. Xiao, H.C. Yang, Y. Shi, K. Chen, S.G. Wang, B.S. Zhang, Q.H. Yang, F. Li, Efficient polysulfide blocker from conductive niobium nitride@graphene for Li-S batteries, J. Electroanal. Chem., 45 (2020) 135-141.

[3] W.L. Cai, G.R. Li, K.L. Zhang, G.N. Xiao, C. Wang, K.F. Ye, Z.W. Chen, Y.C. Zhu, Y.T. Qian, Conductive Nanocrystalline Niobium Carbide as High-Efficiency Polysulfides Tamer for Lithium-Sulfur Batteries, Adv. Funct. Mater., 28 (2018) 1704865.

[4] Y. Luo, N. Luo, W. Kong, H. Wu, K. Wang, S. Fan, W. Duan, J. Wang, Multifunctional Interlayer Based on Molybdenum Diphosphide Catalyst and Carbon Nanotube Film for Lithium-Sulfur Batteries, Small, 14 (2018) 1702853.

[5] J.L. Yang, S.X. Zhao, Y.M. Lu, X.T. Zeng, W. Lv, G.Z. Cao, In-situ topochemical nitridation derivative MoO_2-Mo_2N binary nanobelts as multifunctional interlayer for fast-kinetic Li-Sulfur batteries, Nano Energy, 68 (2020) 104356.

[6] H. Ahn, Y. Kim, J. Bae, Y.K. Kim, W.B. Kim, A multifunctional SnO_2-nanowires/carbon composite interlayer for high- performance lithium-sulfur batteries, Chem. Eng. J., 401 (2020) 126042.

[7] C. Chen, Q.B. Jiang, H.F. Xu, Y.P. Zhang, B.K. Zhang, Z.Y. Zhang, Z. Lin, S.Q. Zhang, Ni/SiO_2/Graphene-modified separator as a multifunctional polysulfide barrier for advanced lithium-sulfur batteries, Nano Energy, 76 (2020) 105033.

[8] N. Wei, J.S. Cai, R.C. Wang, M.L. Wang, W. Lv, H.N. Ci, J.Y. Sun, Z.F. Liu, Elevated polysulfide regulation by an ultralight all-CVD-built ReS_2@N-Doped graphene heterostructure interlayer for lithium-sulfur batteries, Nano Energy, 66 (2019) 104190.

[9] Q. Hu, J. Lu, C. Yang, C. Zhang, J. Hu, S. Chang, H. Dong, C. Wu, Y. Hong, L. Zhang, Promoting Reversible Redox Kinetics by Separator Architectures Based on CoS_2 /HPGC Interlayer as Efficient Polysulfide-Trapping Shield for Li-S Batteries, Small, 16 (2020) 2002046.

[10] T.H. Zhou, W. Lv, J. Li, G.M. Zhou, Y. Zhao, S.X. Fan, B.L. Liu, B.H. Li, F.Y. Kang, Q.H. Yang, Twinborn TiO_2-TiN heterostructures enabling smooth trapping-diffusion-conversion of polysulfides towards ultralong life lithium-sulfur batteries, Energy Environ. Sci., 10 (2017) 1694-1703.

[11] J. Zhu, Y. Liu, L. Zhong, J. Wang, H. Chen, S. Zhao, Y. Qiu, Hybrid TiO-TiO_2 nanoparticle/B-N co-doped CNFs interlayer for advanced Li S batteries, J. Electroanal. Chem., 881 (2021) 114950.

[12] Q.Q. Huang, M.Q. Chen, Z. Su, L.Y. Tian, Y.Y. Zhang, D.H. Long, Rational cooperativity of nanospace confinement and rapid catalysis via hollow carbon nanospheres@Nb-based inorganics for high-rate Li-S batteries, Chem. Eng. J., 411 (2021) 128504.

[13] X. Li, B. Gao, X. Huang, Z. Guo, Q. Li, X. Zhang, P.K. Chu, K. Huo, Conductive Mesoporous Niobium Nitride Microspheres/Nitrogen-Doped Graphene Hybrid with Efficient Polysulfide Anchoring and Catalytic Conversion for High-Performance Lithium-Sulfur Batteries, ACS Appl. Mater. Interfaces, 11 (2019) 2961-2969.

[14] W.N. Ge, L. Wang, C.C. Li, C.S. Wang, D.B. Wang, Y.T. Qian, L.Q. Xu, Conductive cobalt doped niobium nitride porous spheres as an efficient polysulfide convertor for advanced lithium-sulfur batteries, J. Mater. Chem. A, 8 (2020) 6276-6282.

[15] Y. Tao, Y. Wei, Y. Liu, J. Wang, W. Qiao, L. Ling, D. Long, Kinetically-enhanced polysulfide redox reactions by Nb_2O_5nanocrystals for high-rate lithium–sulfur battery, Energy Environ. Sci., 9 (2016) 3230-3239.
[16] Z. Xiao, Z. Yang, L. Zhang, H. Pan, R. Wang, Sandwich-Type NbS_2@S@I-Doped Graphene for High-Sulfur-Loaded, Ultrahigh-Rate, and Long-Life Lithium-Sulfur Batteries, ACS Nano, 11 (2017) 8488-8498.
[17] J.Y. Wang, G.R. Li, D. Luo, Y. Zhao, Y.G. Zhang, G.F. Zhou, L.L. Shui, X. Wang, Amorphous-crystalline-heterostructured niobium oxide as two-in-one host matrix for high-performance lithium-sulfur batteries, J. Mater. Chem. A, 9 (2021) 11160-11167.
[18] D. Luo, Z. Zhang, G. Li, S. Cheng, S. Li, J. Li, R. Gao, M. Li, S. Sy, Y.P. Deng, Y. Jiang, Y. Zhu, H. Dou, Y. Hu, A. Yu, Z. Chen, Revealing the Rapid Electrocatalytic Behavior of Ultrafine Amorphous Defective Nb_2O_{5-x} Nanocluster toward Superior Li-S Performance, ACS Nano, 14 (2020) 4849-4860.